Research Paper

Novel ovarian endometriosis model causes infertility via iron-mediated oxidative stress in mice

Shotaro Hayashi [a,b], Tomoko Nakamura [b], Yashiro Motooka [a], Fumiya Ito [a], Li Jiang [a], Shinya Akatsuka [a], Akira Iwase [c], Hiroaki Kajiyama [b], Fumitaka Kikkawa [b], Shinya Toyokuni [a,d,e,*]

[a] Department of Pathology and Biological Responses, Nagoya University Graduate School of Medicine, 65 Tsurumai-cho, Showa-Ku, Nagoya, 466-8550, Japan
[b] Department of Obstetrics and Gynecology, Nagoya University Graduate School of Medicine, 65 Tsurumai-cho, Showa-Ku, Nagoya, 466-8550, Japan
[c] Department of Obstetrics and Gynecology, Gunma University School of Medicine, 3-39-22, Showa-machi, Maebashi, 371-8511, Japan
[d] Center for Low Temperature Plasma Sciences, Nagoya University, Furo-cho, Chikusa, Nagoya, 484-8601, Japan
[e] Sydney Medical School, The University of Sydney, NSW, Australia

ARTICLE INFO

ABSTRACT

Ovarian endometriosis (OE) provides women of reproductive age with not only severe menstrual pain but also infertility and an increased risk for ovarian carcinogenesis. Whereas peritoneal endometriosis models have been developed with syngeneic implantation of minced uterine tissue and oncogenic *K-ras* allele with conditional *Pten* deletion within ovarian surface epithelium generated preneoplastic endometrial glandular morphology, followed by endometrioid adenocarcinoma, there has been no mouse model of OE similar to human counterparts, applicable to preclinical studies. Here we for the first time established a murine OE model that reveals infertility, and evaluated the involvement of iron catalyzed oxidative stress in the pathogenesis. Minced uterine tissue from female mice was implanted on ovarian surface of syngeneic mice after bursectomy to induce OE. Ectopic growth of endometrium was observed in association with ovary 4 weeks after implantation in 85.7% (12/14) of the operated mice with our protocol. Endometriotic lesions involved intestine, pancreas and peritoneal wall. Fibrosis around the ovary was prominent and increased time-dependently in the OE group. Iron accumulation was significantly increased in the OE group, leading to oxidative stress in each stage of the follicles as evaluated by 4-hydroxy-2-nonenal-modified proteins and 8-hydroxy-2′-deoxyguanosine. Expression of follicle stimulating hormone receptor in the follicles revealed a significant decrease during pre-antral, antral and pre-ovulatory phases in the OE group. Finally, the number of pups was significantly reduced in the OE group in comparison to the controls. This model affords an opportunity to evaluate agents or procedures to counteract ovarian endometriosis in the preclinical settings.

1. Introduction

Endometriosis is a disease that retrograded endometrium grows on the peritoneal cavity. Approximately 10–15% of fertile women are diagnosed as endometriosis [1,2]. Ovarian endometriosis is the most common lesion of endometriosis, which gynecologists frequently detect with sonography [3]. Endometriosis with ovarian lesion may cause infertility [4] and ovarian cancer in addition to dysmenorrhea [5–9]. Endometriosis leads to infertility presumably via iron overload and oxidative stress [10] on follicular growth [11]. However, the molecular

mechanisms how ovarian endometriosis suppresses folliculogenesis is still not elucidated yet. That is partly because it is ethically unacceptable to dissect functional ovaries for basic research from young fertile women with endometrioma.

There have been reports on murine endometriosis models, mimicking the human disease. Mouse models of peritoneal lesions [12] and deep endometriosis [13] were reported. In the previous reports, most of the endometriosis mouse models were surgically induced by homologous transplantation of uterine tissue, based on Sampson's theory [14]. Although this model develops peritoneal cystic lesions of ectopic endometrium, ovarian endometriosis is hardly induced.

ovarian surface under the protection by the bursal membrane. At least two mice models have been developed with genetic engineering; one with oncogenic *K-Ras* and conditional *Pten* deletion within the ovarian surface epithelium gave rise to preneoplastic ovarian lesions with an endometrioid glandular morphology, eventually leading to endometroid ovarian cancer [16]; the other with an *Arid1a* (*AT-rich interactive domain-containing protein 1A*) and *Pik3ca* (*phosphatidylinositol-4, 5-bisphosphate 3-kinase, catalytic subunit alpha*) mutant model of endometrial dysfunction following salpingectomy revealed naturally spread ectopic endometrium on peritoneum and ovary, which was not unfortunately available for long-term observation because the mice died at 17 weeks old [17]. Therefore, there is no report on the murine ovarian endometriosis model, available for research on ovarian function and
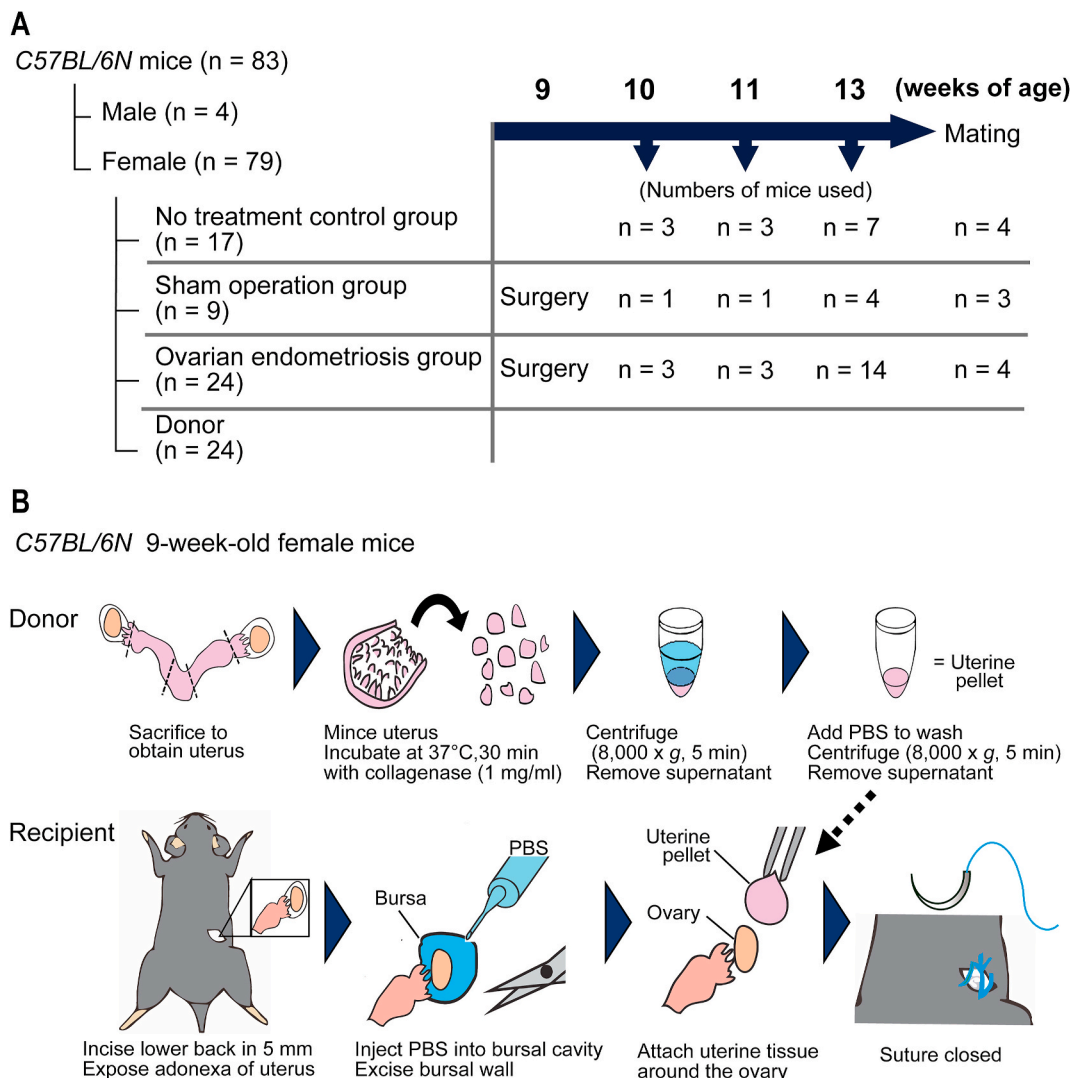

Fig. 1. Protocol to generate the ovarian endometriosis model in mice.
(A) Summary of experimental design. (B) Experimental procedures. *C57BL/6 N* female mice at 9 weeks of age were used. Donor mice were euthanized and the dissected uterus was longitudinally cut and minced at ~0.5 mm in diameter with scissors. Minced uterus was incubated with a collagenase solution (1 mg/ml) for 30 min at 37 °C, which was centrifugated (8000×g, 5 min) to remove supernatant, and resuspended in 100 μl of phosphate-buffered saline (PBS) to be rinsed by an additional centrifugation (8000×g, 5 min). Then, the tissue pellet was used for transplantation. Recipient mice at 9 weeks of age under isoflurane anesthesia received 5 mm bilateral incisions on their lower back and the ovaries were exposed, to which 100 μl of PBS was injected to intra bursal cavity to identify bursal membrane. Then, we cut it off to expose the ovarian surface. A half of uterine pellet was attached on each exposed ovarian surface. The ovaries were pushed back into the peritoneal cavity, followed by suture of the dorsal scissions. Refer to text for details.

Morphologically, mouse or rat ovaries are covered with a special membranous structure called bursa [15], which separates ovaries from peritoneal cavity. Accordingly, ectopic endometrium cannot attach

fertility potential. Accordingly, we decided to devise a novel method to generate a mouse model of ovarian endometriosis that enables the investigation of ovarian function.

Table 1

Experimental conditions for immunohistochemistry.

Target molecule	Supplier	Catalogue number	Immunized host	Dilution	Epitope retrieval solution
CD10 (H-321)	Santa Cruz	sc-9149	Rabbit	1:1000	1
FSH receptor	Proteintech	22665-1-AP	Rabbit	1:1000	2
4-HNE	Bioss Antibodies	BS-6313R	Rabbit	1:1000	1
8-OHdG	Bioss Antibodies	BS-1278R	Rabbit	1:1500	1

Refer to text for details.

We performed several new procedures to establish our model of murine ovarian endometriosis, including the excision of ovarian bursa and transplantation of dissected syngeneic endometrial tissues in pellets on the ovarian surface. As a primary goal, we finally established a novel ovarian endometriosis model in mice which allows evaluation of ovarian dysfunction. We could further observe iron-catalyzed oxidative stress on follicular maturation and infertility in this model. The usefulness of this model would be discussed.

2. Materials and methods

2.1. Animal experiments

All the protocols of animal experiments were approved by the Animal Experimental Committee of Nagoya University Graduate School of Medicine (31452). *C57*BL/*6 N* female mice (8 weeks of age) were purchased from Japan SLC, Inc. (Hamamatsu, Shizuoka, Japan). A total of 83 mice (79 females and 4 males) were used. The experimental design is summarized in Fig. 1A. The care and handling of animals were in accordance with the National Institutes of Health guidelines. Before starting the experiments, the animals were acclimatized for 7 days and were maintained at 23–25 °C with a 12-h dark/light cycle and with standard chow (CE-2; CLEA Japan, Inc., Tokyo, Japan) and water under specific pathogen-free condition. Cages were changed weekly.

2.2. Donor mice

Donor female mice of 9-weeks of age (n = 24 in total) were euthanized to obtain uterine tissue, which was dissected *en bloc* after euthanasia and was cleaned of supplementary fibroadipose tissues in phosphate-buffered saline (PBS). The uterus was cut longitudinally with a linear incision and minced (approximately 0.5 mm in diameter) with scissors under laminar flow (Fig. 1B). The uterus was incubated with collagenase solution (1 mg/ml; FUJIFILM Wako Pure Chemical Corporation, Osaka, Japan) for 30 min at 37 °C. Tissue was then centrifuged at $8000 \times g$, 5 min to remove supernatant, and was resuspended in 100 μl of PBS, followed by washing with additional centrifugation ($8000 \times g$, 5 min) to remove collagenase. Then, the pellet of uterine tissue was immediately used for transplantation.

2.3. Recipient mice and surgery protocol

Twenty-four female mice were used as recipients of uterine pellets for ovarian endometriosis (OE) group (Fig. 1A). Mice underwent uterine transplantation after a week of acclimatized period. Induction and maintenance of systemic anesthesia were achieved with isoflurane (3% for induction; 2.5% for maintenance). Incisions of 5–7 mm were performed to bilateral back skin and muscle layers to search for ovaries. PBS (100 μl) was injected into the ovarian bursal space using a syringe with 26-gauge needle to detect and clarify bursal membrane (Fig. 1B). Bursal cyst wall was then extended with suturing needle and peeled off with scissors and tweezers to expose ovarian surface. A half of uterine tissue pellet prepared from one donor female mouse was placed equally over each surface of bilateral ovaries. Ovaries with attached uterine pellet were then pushed back into the peritoneal cavity. Skin and muscle incisions were sutured with a Z-suturing, using 3-0 Vicryl (Ethicon US).

Table 2

Number of ovarian follicles analyzed with immunohistochemistry.

Target molecule	Control	Sham-operated	Ovarian endometriosis
Number of model mice	7	4	7
4-HNE			
Primordial	103	35	49
Primary	36	11	29
Secondary	54	15	39
Pre-antral	45	11	38
Antral	22	10	11
8-OHdG			
Primordial	58	19	73
Primary	67	49	46
Secondary	71	31	37
Pre-antral	45	35	49
Antral	29	9	20
FSH receptor			
Pre-antral	25	25	16
Antral	26	12	24
Pre-ovulatory	12	4	4

Refer to text for details.

Nine female mice received sham operation, including anesthesia, bilateral back incision and PBS injection into bursal cavity but without uterine transplantation.

2.4. Tissue collection and pathological analysis

Mice were euthanized at the age of 10, 11 or 13 weeks to collect ovaries and other lesions (Fig. 1A). Tissues were fixed immediately after dissection in 10% (w/v) phosphate-buffered formalin and embedded in paraffin for pathological analyses. Hematoxylin & eosin staining, Masson trichrome staining for detecting collagen fibers and Berlin blue staining for detecting excess iron (hemosiderin) were performed. Colored areas after each staining inside ovary were quantitated with Image J software (https://imagej.nih.gov/ij/). The average values were calculated based on colored area (%) of randomly selected at least 5 magnified images in each mouse, which were compared among the three groups.

2.5. Immunohistochemistry

Immunohistochemical staining was performed with a Leica Bond Max automated system (Leica, Bannockburn, IL) according to the manufacturer's instructions. Immunostaining was preceded for 30 min either by BOND Epitope Retrieval Solution 1 (AR9961) or 2 (AR9640), depending on the primary antibody. The primary antibodies were diluted at proper concentrations with BOND Primary Antibody Diluent (AR9352). Primary antibodies and the experimental conditions used are summarized in Table 1.

2.6. Quantitative analysis of oxidative stress

4-Hydroxy-2-nonenal (4-HNE) is one of the most specific lipid peroxidation products in iron-catalyzed Fenton reaction [18–20]. We used a rabbit polyclonal antibody against HNE-modified proteins as anti-4-HNE antibody (BS-6313R; Bioss Antibodies Inc., Woburn, MA). 4-HNE positivity of ovarian follicles was evaluated by quantifying %
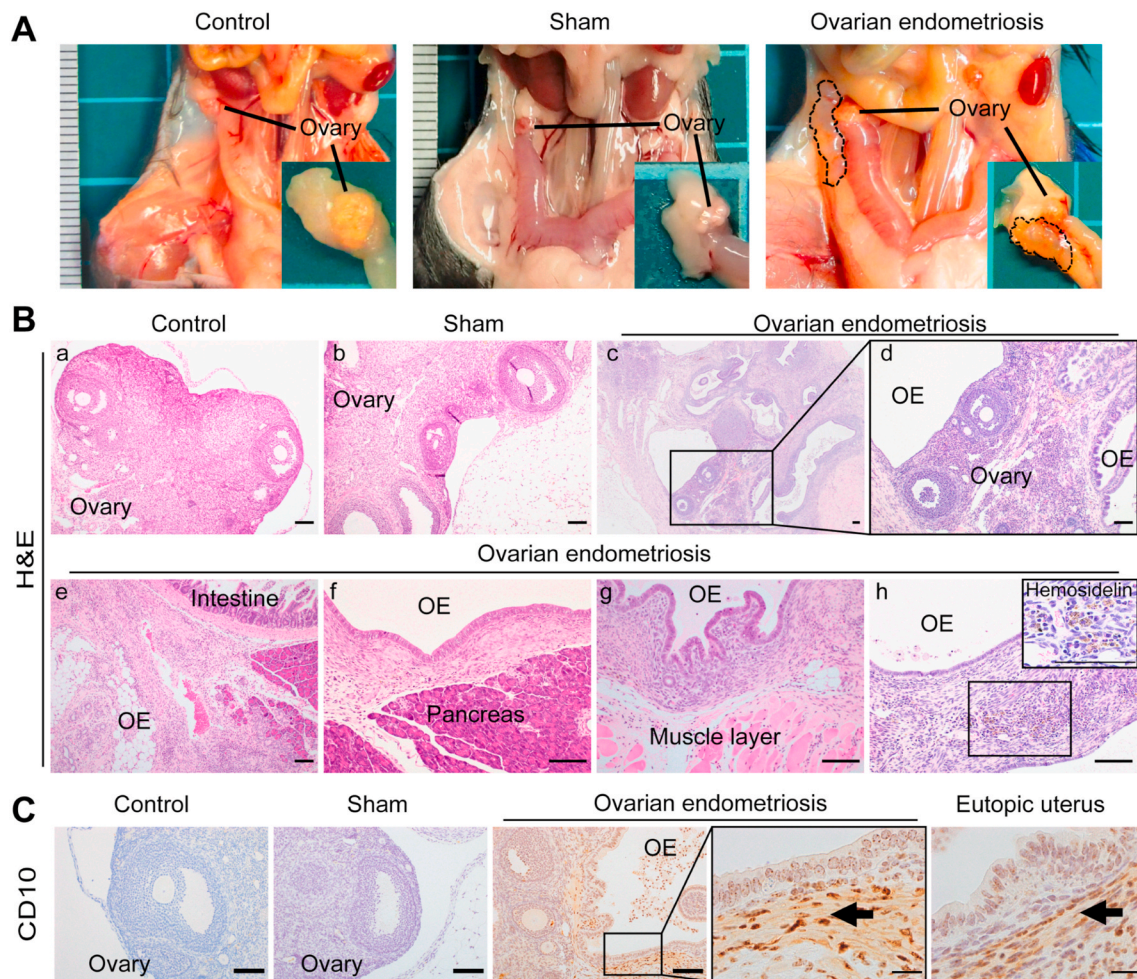
Fig. 2. Analysis of the novel ovarian endometriosis model.

Ectopic endometrial cystic growth was visible in association with ovary 4 weeks after the transplantation in the OE (ovarian endometriosis) group. The mice in each group were euthanized 1, 2 and 4 weeks after the procedure and the lesions were evaluated. (A) Single or multiple cystic lesions were observed in association with the ovaries of the OE group whereas those in the other groups were not altered. Adhesion was evident between the endometriotic cysts and other adjoining organs, such as intestine, pancreas and abdominal wall. (B, C) Histology confirmed endometriosis. The ovarian cystic lesions of the OE group consisted of single-layered epithelium and underlying stoma with hemosiderin accumulation and CD10 immunopositivity in the endometriotic stroma (arrows; bar = 100 μm). Refer to text for details.

area of immunopositivity of each follicular area with Image J (threshold 170). We also used a rabbit polyclonal antibody (BS-1278R; Bioss Antibodies Inc.) directed against 8-hydroxy-2′-deoxyguanosine (8-OHdG), a major product of DNA base oxidation [19,21]. 8-OHdG-positive granulosa cells were counted (% positive cells/total granulosa cells in each follicle). Immunopositivity was evaluated for the three groups at all the follicular stages; primordial, primary, secondary, pre-antral and antral follicles (Table 2), as described previously [22].

2.7. Quantitative analysis of FSH receptor

Expression of follicle stimulating hormone receptor (FSHR) was compared among the three groups with immunohistochemistry. We performed this study only for pre-antral, antral and pre-ovulatory stages (Table 2) because the growth of ovarian follicles depends on FSH from the pre-antral stage [23,24]. Immunopositivity of FSHR was quantified as described above for 4-HNE (Table 2).

2.8. Evaluation of fertility

Fertility was tested in the model animals as described previously [25] with a modification. Nine-week-old female mice were enrolled in

the C (n = 4), S (n = 3) or OE (n = 4) groups for the evaluation of fertility. Mating was started at 13 weeks with male mice of the same age. One or two test female mice and one male mouse were placed together in a cage. In order to ensure a successful conception, male mice were allowed to stay in the designated cage for 4–7 days and were exchanged between cages until female mice were confirmed as pregnant. All the pregnant mice were confirmed by inspection and palpation. We finally euthanized the pregnant mice between the 10th-18th day of conception prior to spontaneous delivery to accurately count embryos in order to avoid still birth, predation by a mother and any factors to reduce the baby number.

2.9. Statistical analysis

Statistical analyses were performed using one-way analysis of variance (ANOVA) and an unpaired t-test with GraphPad Prism 5 software (San Diego, CA). Differences were considered significant when $P < 0.05$. The data are expressed as the means ± SEM, unless otherwise specified.
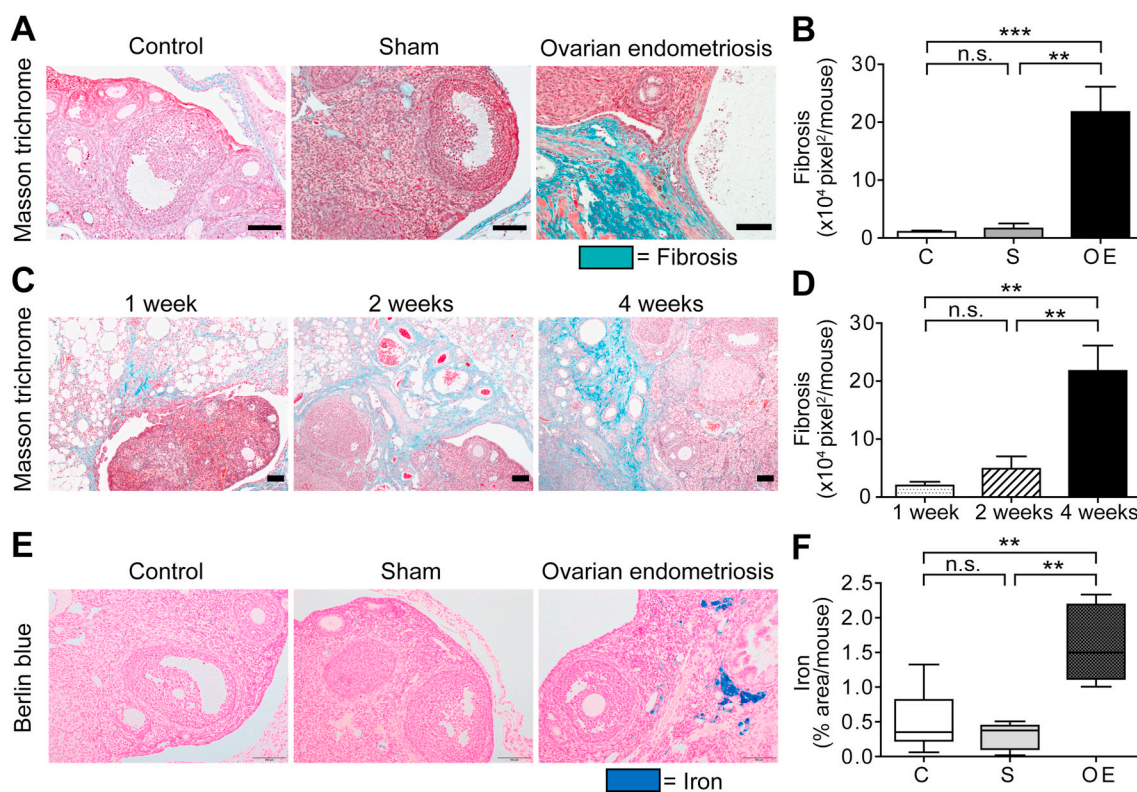
Fig. 3. Fibrosis and iron accumulation in ovarian endometriosis.
(A) Fibrotic area was significantly increased in the OE group in comparison to C and S group. (B) Quantitative analysis of A. (C) Fibrosis was time-dependently increased in the OE group. (D) Quantitative analysis of C. (E) Berlin Blue staining revealed hemosiderin deposition only in the OE group at 4 weeks. (F) Quantitative analysis of E (means ± SEM; **, $P < 0.01$; ***, $P < 0.001$; n. s., not significant; bar = 100 μm). Refer to text for details. . (For interpretation of the references to color in this figure legend, the reader is referred to the Web version of this article.)

3. Results

3.1. Novel murine model of ovarian endometriosis

The mice of all the groups were euthanized 1, 2 and 4 weeks after the operation (at the ages of 10, 11 and 13 weeks, respectively) and endometriotic lesions were evaluated. Single or multiple cystic lesions were recognized at 4 weeks in association of bilateral ovaries only in 85.7% (12/14; bilateral ovarian lesion in 8 mice and one side in 4 mice) of the OE group whereas ovaries in the other groups showed no alterations (Fig. 2A). The cystic lesions contained clear light-yellow fluid as observed in the previous reports on peritoneal endometriosis models [12]. Much smaller lesions were confirmed at 1 and 2 weeks of the OE group, and the progression of the lesion was time-dependent.

Histological examination demonstrated the ovarian cystic lesions as ovarian endometriosis. Cystic lesions of the OE group consisted with single-layered columnar epithelium without cilia, concomitant with underlying stromal tissue. Whereas the shapes of ovaries in the C and S groups were normal (Fig. 2 Bab), the structures of ovaries in the OE group were changed by invasive endometriotic lesion (Fig. 2Bcd). Furthermore, in the OE group, endometriotic lesion associated with ovaries infiltrated into the neighboring tissues, such as intestine (Fig. 2Be), pancreas (Fig. 2Bf) or peritoneal wall (Fig. 2Bg), concomitant with endometriotic stroma. Of note, the endometriotic stroma of this novel OE model contained hemosiderin granules (Fig. 2Bh), which is often recognized in the human endometriotic lesion [9,26]. We also confirmed immunopositivity for CD10 in the endometriotic stroma of these lesions (Fig. 2C).

3.2. Fibrosis and iron deposition in endometriotic lesions

One of the characteristics of endometriosis is fibrosis. We then evaluated fibrogenesis of endometriotic lesions with Masson trichrome staining. In the OE group, green fibrotic areas in association with the endometriotic stroma were significantly increased in comparison to the C or S groups (Fig. 3AB), which progressed time-dependently (Fig. 3CD). Iron deposition in endometriotic stroma is another feature of endometriosis. In the OE group, iron accumulation was significantly higher than the other groups at 4 weeks (Fig. 3EF).

3.3. Oxidative stress in ovarian follicles in endometriotic lesions

We evaluated endometriosis-associated oxidative stress on ovarian follicles at 4 weeks with two distinct oxidative stress markers, 4-HNE and 8-OHdG. The number of follicles we evaluated is summarized in Table 2. Representative data of different maturation stages with 4-HNE immunohistochemistry are summarized in Fig. 4A. In the primordial follicles, 4-HNE levels were higher in the OE group than the other two groups (C vs OE, $P < 0.001$; S vs OE, $P < 0.001$) (Fig. 4B). In the primary and secondary follicles, 4-HNE levels were not significantly different among the three groups (Fig. 4CD). In the pre-antral follicles, 4-HNE levels of follicles in the OE group were significantly higher than the C and S groups (Fig. 4E; C vs OE, $P < 0.001$; S vs OE, $P < 0.01$; C vs S, $P = 0.6206$). The results were similar in the antral follicles (Fig. 4F; C vs OE, $P < 0.05$; S vs OE, $P < 0.01$; C vs S, $P = 0.2150$).

Representative data of the follicular cells at 4 weeks with 8-OHdG immunohistochemistry are shown in Fig. 5A. In every follicular stage studied, fraction of 8-OHdG positive granulosa cells was significantly higher in the OE group than the C and S groups (primordial: C vs OE, $P < 0.01$; S vs OE, $P < 0.05$; C vs S, $P = 0.3152$ [Fig. 5B]; primary: C vs OE, P
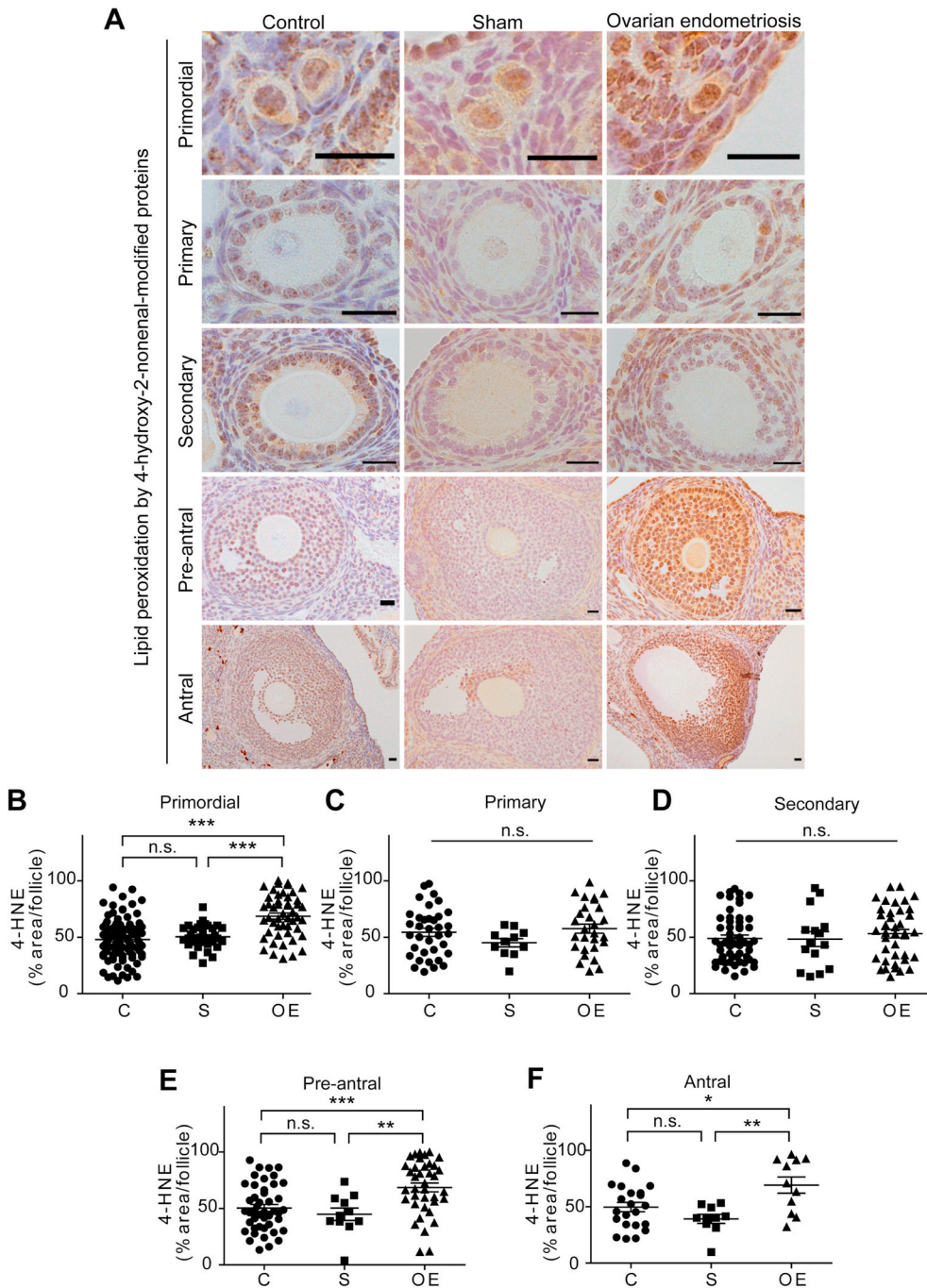
Fig. 4. High lipid peroxidation levels as evaluated by 4-hydroxy-2-nonenal-modified proteins (4-HNE) in the primordial, pre-antral and antral stages of ovarian follicles of ovarian endometriosis.

(A) Representative 4-HNE immunohisto-chemical results of ovarian follicles in each group. Premordial

preantral and antral follicles revealed higher levels of 4-HNE in the OE group in comparison to C and S groups. (B–

F) Quantitative analysis of each follicular stage of the ovary (means ± SEM; *, $P <$ 0.05; **, $P < 0.01$; ***, $P < 0.001$; n. s., not significant; bar = 20 μm). Refer to text for details.

< 0.01; S *vs* OE, $P < 0.01$; C *vs* S, $P = 0.2303$ [Fig. 5C]; secondary: C *vs* OE, $P < 0.01$; S *vs* OE, $P < 0.05$; C *vs* S, $P = 0.9273$ [Fig. 5D]; pre-antral: C *vs* OE; $P < 0.01$, S *vs* OE; $P < 0.05$, C *vs* S; $P = 0.3524$ [Fig. 5E]; antral: C *vs* OE; $P < 0.01$, S *vs* OE; $P < 0.05$, C *vs* S; $P = 0.7619$ [Fig. 5F]).

3.4. Endometriosis reduced FSHR expression in ovary

FSH is necessary for the follicular growth and oocyte maturation prior to ovulation through the steroid hormone synthesis via FSHR. The representative data panels at 4 weeks are summarized in Fig. 6A. FSHR expression of follicles in the pre-antral, antral and pre-ovulatory stages was significantly lower in the OE group in comparison to the C or S groups (pre-antral: C *vs* OE, $P < 0.001$; S *vs* OE; $P < 0.01$, C *vs* S; $P = 0.1624$ [Fig. 6B]; antral: C *vs* OE, $P < 0.001$; S *vs* OE, $P < 0.001$; C *vs* S, P

$= 0.9624$ [Fig. 6C]; pre-ovulatory: C *vs* OE, $P < 0.01$; S *vs* OE, $P < 0.05$; C *vs* S, $P = 0.2493$ [Fig. 6D]).

3.5. Endometriosis induced a significant decrease in fetuses at fertilization

We examined the difference in the number of pups obtained in each group. We obtained a total of 36, 27 and 9 pups from the mother mice in the C (n = 4), S (n = 3) and OE (n = 4) groups, respectively. Representative pictures are shown in Fig. 7A. Mean numbers (and range) of the babies were 9.0 (6–12), 9.0 (7–11) and 2.3 (1–3) in the groups C, S and OE, respectively. The average number of conceived babies was significantly lower in the OE group in comparison to the other two groups (Fig. 7B; C *vs* S, $P = 0.8544$; C *vs* OE, $P < 0.05$; S *vs* OE, $P < 0.05$).
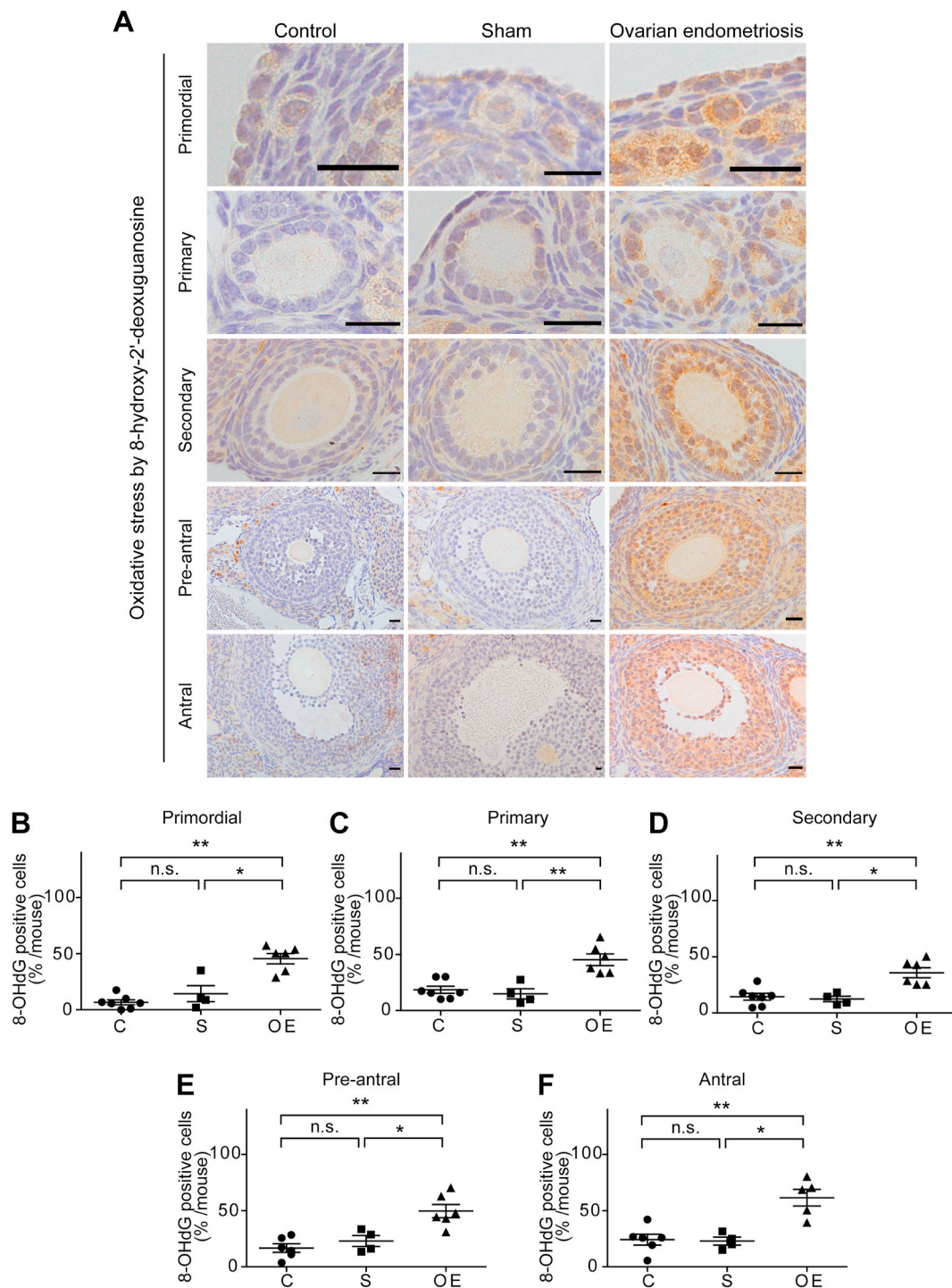
Fig. 5. High levels of nuclear 8-hydroxy-2′-deoxyguanosine (8-OHdG) in the granulosa cells during the whole follicular stages of ovarian endometriosis.
(A) Representative 8-OHdG immunohistochemical results of ovarian follicles in each group. Follicles of all the stages revealed significantly higher levels of nuclear 8-OHdG in the OE group in comparison to C and S groups. (B-
F) Quantitative analysis of each follicular stage of the ovary (means ± SEM; *, $P < 0.05$; **, $P < 0.01$; n. s., not significant; bar = 20 μm). Refer to text for details.

4. Discussion

Here we have established a novel ovarian endometriosis model in *wild-type* mice with high reproducibility of 85.7%. As far as we know, this is the first model for ovarian endometriosis to be used for various preclinical studies. The distinctive procedures of our model are the removal of ovarian bursa and transplantation of syngeneic uterine tissue as a pellet. Though we tried intra-bursal injection of uterine tissue suspension without bursal removal, we observed no endometriotic lesion on the ovarian surface (unpublished data). We suspect that there are two reasons for this negative result; 1) minced uterine tissue was too large to pass through the needle pore of 26-gauge; 2) small numbers of tiny pieces of uterine tissue might not have enough potential to develop lesions. Further, we also tried intra-bursal uterine tissue injection suspended in atelocollagen acidic solution (#IPC-50, KOKEN, Japan) used for 3D-culture, but no endometriotic lesion was found as well
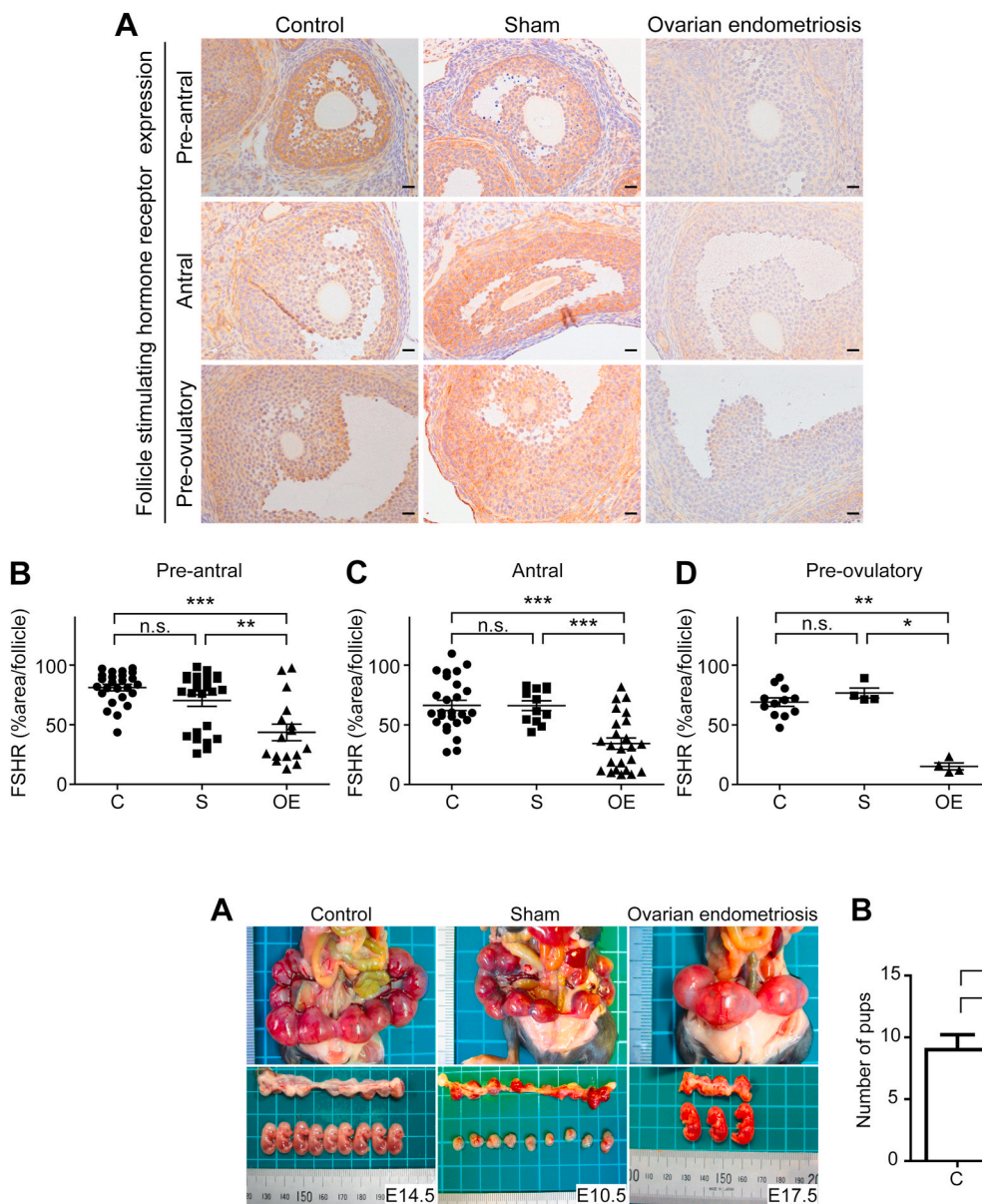
Fig. 6. Follicle stimulating hormone receptor (FSHR) expression was significantly decreased in ovarian endometriosis.

(A) Representative FSHR immunohisto-chemical results of ovarian follicles at the preantral, antral and preovulatory stages in each group. Follicles of all the stages examined revealed significantly lower levels of FSHR in the OE group in comparison to C and S groups. (B-

F) Quantitative analysis of each follicular stage of the ovary (means ± SEM; *, $P < 0.05$; **, $P < 0.01$; ***, $P < 0.001$; n. s., not significant; bar = 20 μm). Refer to text for details.

Fig. 7. Subfertility in the ovarian endometriosis model.
(A) Representative results of mating experiments in each group. The number of pups in the OE group (n = 4) was significantly lower than those in C (n = 3) and S (n = 4) groups. (B) Quantitative analysis of A (means ± SEM; *, $P < 0.05$). Refer to text for details.

(unpublished data). The idea of collagenase digestion and pellet formation were based on primary cell culture techniques [27,28]. Pellets of uterine tissue were easy to hold with tweezers when putting it specifically on ovarian surface rather than endometrial homogenate injection. Our method is also cost friendly because it requires only equipment that we routinely use in the laboratory, and is easy because pre-/post-operative estradiol administration is not required in comparison to previous methods [12,13].

Our model of ovarian endometriosis induced significant structural alterations in the ovary with infiltration of the lesion to the nearby tissues and organs, such as intestine, pancreas, and abdominal wall. We observed that ovarian surface was invaded and replaced by endometriotic stroma with massive collagen production, which allowed less space for the ovarian follicles to grow. Iron deposition was detected in the induced ovarian endometriotic stromal area. Notably, it has been suggested that excess iron may promote the development of ovarian endometriosis [12]. Furthermore, iron and oxidative stress has been reported as one of the major factors of subfertility in ovarian

endometriosis [29,30]. We could demonstrate in our model that an increased level of oxidative stress in the ovarian follicles was associated with decrease in FSHR expression and decrease in the number of fetuses at conception. As we previously reported that endometriotic stromal cells reveal high iron affinity [31], ovarian endometriosis is considered as a supplier of excess iron, leading to a negative effect on ovarian folliculogenesis [9] through catalyzing the generation of reactive oxygen species [32,33]. In our data, 4-HNE [34] was significantly increased in the primordial, preantral and antral follicles of the OE group. As previously reported, 4-HNE was induced by cisplatin- or paclitaxel-induced oxidative stress in the primordial follicles [35]. Follicles in the preantral and antral follicle stages contain more cholesterol to synthesize steroid hormones [36], which may become the target of lipid peroxidation.

Although we did not study the molecular mechanism how oxidative stress suppressed FSHR expression, we believe that there are underlying epigenetic regulation of *FSHR* gene as suggested by previous reports. For instance, oxidative stress is reported as a cause of DNA methylation or histone acetylation [37]. Moreover, epigenetic mechanisms regulate

FSHR expression [38]. Further studies are now in progress to test this hypothesis.

In the mating experiments, mice with ovarian endometriosis presented low fertility potential. In our ovarian endometriosis model, oxidative stress caused FSHR suppression and reduced follicular growth, resulting eventually in the reduced number of pups. An association between oxidative stress and infertility has been reported both from the clinical and basic points of view [11]. Although no medicine for oxidative stress-associated infertility has been developed yet, our mouse model may contribute to screening new drugs to recover infertility due to oxidative stress induced by ovarian endometriosis.

Clinically, ovarian endometriosis is a risk for ovarian cancer [9,26, 39]. Whereas the precise molecular mechanisms that endometriosis generates ovarian cancer is still unclear, one major hypothesis is persistent oxidative stress via the excess iron [10,40] associated with monthly hemorrhage inside and nearby ovary. Hopefully, our ovarian endometriosis mouse model can also contribute to elucidating ovarian endometriosis-associated carcinogenic mechanisms, which requires much longer-term observation of a few years. Further experiments would soon be started in our laboratory.

In conclusion, we have for the first time established a reproducible ovarian endometriosis model with infertility in mice. We demonstrated in this new model that ovarian endometriosis accompanying fibrosis leads to iron-catalyzed oxidative stress in follicles and the resultant reduced FSHR expression and subfertilization. We hope that this model would contribute to the preclinical studies to find a strategy to cure endometriosis-associated infertility, including those using non-thermal plasma [41].

Author contributions

SH, TN and ST conceived and designed the experiments. SH, YM, FI, LJ and SA collected and analyzed the data. SH, TN, AI, HK, FK and ST interpreted the whole results. SH and ST wrote the manuscript.

Declaration of competing interest

The authors have nothing to disclose.

Acknowledgements

References

[1] R.O. Burney, L.C. Giudice, Pathogenesis and pathophysiology of endometriosis, Fertil. Steril. 98 (3) (2012) 511–519.

[2] M.L. Macer, H.S. Taylor, Endometriosis and infertility: a review of the pathogenesis and treatment of endometriosis-associated infertility, Obstet. Gynecol. Clin. N. Am. 39 (4) (2012) 535–549.

[3] B.G. Collins, A. Ankola, S. Gola, K.L. McGillen, Transvaginal US of endometriosis: Looking beyond the endometrioma with a dedicated protocol, Radiographics 39 (5) (2019) 1549–1568.

[4] D. de Ziegler, B. Borghese, C. Chapron, Endometriosis and infertility: pathophysiology and management, Lancet 376 (9742) (2010) 730–738.

[5] E. Somigliana, P. Vigano, F. Parazzini, S. Stoppelli, E. Giambattista, P. Vercellini, Association between endometriosis and cancer: a comprehensive review and a critical analysis of clinical and epidemiological evidence, Gynecol. Oncol. 101 (2) (2006) 331–341.

[6] K. Yamaguchi, M. Mandai, S. Toyokuni, J. Hamanishi, T. Higuchi, K. Takakura, S. Fujii, Contents of endometriotic cysts, especially the high concentration of free iron, are a possible cause of carcinogenesis in the cysts through the iron-induced persistent oxidative stress, Clin. Canc. Res. 14 (1) (2008) 32–40.

[7] M. Hamdan, G. Dunselman, T.C. Li, Y. Cheong, The impact of endometrioma on IVF/ICSI outcomes: a systematic review and meta-analysis, Hum. Reprod. Update 21 (6) (2015) 809–825.

[8] S. Toyokuni, Oxidative stress as an iceberg in carcinogenesis and cancer biology, Arch. Biochem. Biophys. 595 (2016) 46–49.

[9] H. Kajiyama, S. Suzuki, M. Yoshihara, S. Tamauchi, N. Yoshikawa, K. Niimi, K. Shibata, F. Kikkawa, Endometriosis and cancer, Free Radic. Bio.l Med. 133 (2019) 186–192.

[10] S. Toyokuni, I. Yanatori, Y. Kong, H. Zheng, Y. Motooka, L. Jiang, Ferroptosis at the crossroads of infection, aging and cancer, Canc. Sci. 111 (8) (2020) 2665–2671.

[11] X. Lin, Y. Dai, X. Tong, W. Xu, Q. Huang, X. Jin, C. Li, F. Zhou, H. Zhou, X. Lin, D. Huang, S. Zhang, Excessive oxidative stress in cumulus granulosa cells induced cell senescence contributes to endometriosis-associated infertility, Redox Biol 30 (2020), 101431.

[12] S. Defrere, A. Van Langendonckt, S. Vaesen, M. Jouret, R. Gonzalez Ramos, D. Gonzalez, J. Donnez, Iron overload enhances epithelial cell proliferation in endometriotic lesions induced in a murine model, Hum. Reprod. 21 (11) (2006) 2810–2816.

[13] D. Yan, X. Liu, S.W. Guo, The establishment of a mouse model of deep endometriosis, Hum. Reprod. 34 (2) (2019) 235–247.

[14] J.H. Ridley, The validity of Sampson's theory of endometriosis, Am. J. Obstet. Gynecol. 82 (1961) 777–782.

[15] T. Motohara, S. Masuko, T. Ishimoto, T. Yae, N. Onishi, T. Muraguchi, A. Hirao, Y. Matsuzaki, H. Tashiro, H. Katabuchi, H. Saya, O. Nagano, Transient depletion of p53 followed by transduction of c-Myc and K-Ras converts ovarian stem-like cells into tumor-initiating cells, Carcinogenesis 32 (11) (2011) 1597–1606.

[16] D.M. Dinulescu, T.A. Ince, B.J. Quade, S.A. Shafer, D. Crowley, T. Jacks, Role of K-ras and Pten in the development of mouse models of endometriosis and endometrioid ovarian cancer, Nat. Med. 11 (1) (2005) 63–70.

[17] M.R. Wilson, J. Holladay, R.L. Chandler, A mouse model of endometriosis mimicking the natural spread of invasive endometrium, Hum. Reprod. 35 (1) (2020) 58–69.

[18] S. Toyokuni, X.P. Luo, T. Tanaka, K. Uchida, H. Hiai, D.C. Lehotay, Induction of a wide range of C2-12 aldehydes and C7-12 acyloins in the kidney of Wistar rats after treatment with a renal carcinogen, ferric nitrilotriacetate, Free Radic. Biol. Med. 22 (1997) 1019–1027.

[19] S. Toyokuni, The origin and future of oxidative stress pathology: from the recognition of carcinogenesis as an iron addiction with ferroptosisresistance to non-thermal plasma therapy, Pathol. Int. 66 (5) (2016) 245–259.

[20] F. Ito, I. Yanatori, Y. Maeda, K. Nimura, S. Ito, T. Hirayama, H. Nagasawa, N. Kohyama, Y. Okazaki, S. Akatsuka, S. Toyokuni, Asbestos conceives Fe(II)-dependent mutagenic stromal milieu through ceaseless macrophage ferroptosis and β-catenin induction in mesothelium, Redox Biol 36 (2020), 101616.

[21] S. Toyokuni, T. Mori, M. Dizdaroglu, DNA base modifications in renal chromatin of Wistar rats treated with a renal carcinogen, ferric nitrilotriacetate, Int. J. Canc. 57 (1994) 123–128.

[22] M. Myers, K.L. Britt, N.G. Wreford, F.J. Ebling, J.B. Kerr, Methods for quantifying follicular numbers within the mouse ovary, Reproduction 127 (5) (2004) 569–580.

[23] N. Rimon-Dahari, L. Yerushalmi-Heinemann, L. Alyagor, N. Dekel, Ovarian folliculogenesis, results Probl, Cell Differ. 58 (2016) 167–190.

[24] D. Dewailly, G. Robin, M. Peigne, C. Decanter, P. Pigny, C. Catteau-Jonard, Interactions between androgens, FSH, anti-Mullerian hormone and estradiol during folliculogenesis in the human normal and polycystic ovary, Hum. Reprod. Update 22 (6) (2016) 709–724.

[25] M.A. Bilotas, C.N. Olivares, A.G. Ricci, J.I. Baston, T.S. Bengochea, G.F. Meresman, R.I. Baranao, Interplay between endometriosis and pregnancy in a mouse model, PloS One 10 (4) (2015), e0124900.

[26] S. Toyokuni, Role of iron in carcinogenesis: cancer as a ferrotoxic disease, Canc. Sci. 100 (1) (2009) 9–16.

[27] H. Nakanishi, S. Takeuchi, K. Kato, S. Shimizu, K. Kobayashi, M. Tatematsu, T. Shirai, Establishment and characterization of three androgen-independent, metastatic carcinoma cell lines from 3,2'-dimethyl-4-aminobiphenyl-induced prostatic tumors in F344 rats, Jpn. J. Canc. Res. 87 (1996) 1218–1226.

[28] A. Iwase, H. Ando, T. Nagasaka, D. Shibata, T. Harata, Y. Shimomura, M. Goto, F. Kikkawa, Neutral endopeptidase expressed by decidualized stromal cells suppresses akt phosphorylation and deoxyribonucleic acid synthesis induced by endothelin-1 in human endometrium, Endocrinology 147 (11) (2006) 5153–5159.

[29] H. Kobayashi, Y. Yamashita, A. Iwase, Y. Yoshikawa, H. Yasui, Y. Kawai, K. Uchida, N. Uno, S. Akatsuka, T. Takahashi, F. Kikkawa, S. Toyokuni, The ferroimmunomodulatory role of ectopic endometriotic stromal cells in ovarian endometriosis, Fertil. Steril. 98 (2) (2012) 415–422, e1-12.

[30] E.J. Park, U. Jeong, Y. Kim, B.S. Lee, M.H. Cho, Y.S. Go, Deleterious effects in reproduction and developmental immunity elicited by pulmonary iron oxide nanoparticles, Environ. Res. 152 (2017) 503–513.

[31] M. Mori, F. Ito, L. Shi, Y. Wang, C. Ishida, Y. Hattori, M. Niwa, T. Hirayama, H. Nagasawa, A. Iwase, F. Kikkawa, S. Toyokuni, Ovarian endometriosis-associated stromal cells reveal persistently high affinity for iron, Redox Biol 6 (2015) 578–586.

[32] S. Toyokuni, Novel aspects of oxidative stress-associated carcinogenesis, Antioxidants Redox Signal. 8 (7–8) (2006) 1373–1377.

[33] W.H. Koppenol, R.H. Hider, Iron and redox cycling. Do's and don'ts, Free Radic. Biol. Med. 133 (2019) 3–10.

[34] K. Uchida, 4-Hydroxy-2-nonenal: a product and mediator of oxidative stress, Prog. Lipid Res. 42 (4) (2003) 318–343.

[35] Y. Qin, A. Iwase, T. Murase, Bayasula, C. Ishida, N. Kato, T. Nakamura, S. Osuka, S. Takikawa, M. Goto, T. Kotani, F. Kikkawa, Protective effects of mangafodipir against chemotherapy-induced ovarian damage in mice, Reprod. Biol. Endocrinol. 16 (1) (2018), 106.

[36] L. Casarini, P. Crepieux, Molecular mechanisms of action of FSH, Front. Endocrinol. 10 (2019), 305.

[37] Y.J. Menezo, E. Silvestris, B. Dale, K. Elder, Oxidative stress and alterations in DNA methylation: two sides of the same coin in reproduction, Reprod. Biomed. Online 33 (6) (2016) 668–683.

[38] K. Shimizu, T. Nakamura, Bayasula, N. Nakanishi, Y. Kasahara, T. Nagai, T. Murase, S. Osuka, M. Goto, A. Iwase, F. Kikkawa, Molecular mechanism of FSHR expression induced by BMP15 in human granulosa cells, J. Assist. Reprod. Genet. 36 (6) (2019) 1185–1194.

[39] S.V. Torti, F.M. Torti, Iron and cancer: more ore to be mined, Nat. Rev. Canc. 13 (5) (2013) 342–355.

[40] S. Toyokuni, F. Ito, K. Yamashita, Y. Okazaki, S. Akatsuka, Iron and thiol redox signaling in cancer: an exquisite balance to escape ferroptosis, Free Radic. Biol. Med. 108 (2017) 610–626.

[41] C. Ishida, M. Mori, K. Nakamura, H. Tanaka, M. Mizuno, M. Hori, A. Iwase, F. Kikkawa, S. Toyokuni, Non-thermal plasma prevents progression of endometriosis in mice, Free Radic. Res. 50 (10) (2016) 1131–1139.